

Polarization Rotation, Switching and E-T phase diagrams of BaTiO₃: A Molecular Dynamics Study

Jaita Paul¹, Takeshi Nishimatsu,² Yoshiyuki Kawazoe² and Umesh V. Waghmare¹

¹*TSU, Jawaharlal Nehru Centre for Advanced Scientific Research,*

Jakkur PO Bangalore 560 064 India

²*Institute for Materials Research, Tohoku University, Sendai 980-8577, Japan*

Abstract

We use molecular dynamics simulations to understand the mechanisms of polarization switching in ferroelectric BaTiO₃ achieved with external electric field. For tetragonal and orthorhombic ferroelectric phases, we determine the switching paths, and show that polarization rotation through intermediate monoclinic phases (a) facilitates switching at low fields (b) is responsible for a sharp anisotropy in polarization switching. We develop understanding of this through determination of detailed electric field-temperature phase diagrams, that are fundamental to technological applications based on electromechanical and switching response of ferroelectrics.

PACS numbers:

Ferroelectric (FE) materials exhibit spontaneous electric polarization whose magnitude and direction depend sensitively on temperature, pressure and electric field[1]. They are technologically very important because of two of their properties: (a) large electromechanical coupling that is exploited in their applications as sensors and actuators in micro-electromechanical systems [1], and (b) switchability of their polarization from one state to another with applied field, that makes them useful in non-volatile memory devices like ferroelectric random access memories (FeRAMs)[2]. Fundamental understanding of the mechanisms responsible for these properties in the bulk crystals is essential to development of ferroelectrics with improved properties and their use in nano-scale devices.

Direction of spontaneous polarization is typically along a crystallographic direction. For example, tetragonal, orthorhombic and rhombohedral ferroelectric states are characterized by polarization along [001], [110] and [111] directions, respectively. Polarization rotation[3] from a rhombohedral state towards a tetragonal one through an intermediate monoclinic phase was shown to be responsible for an ultrahigh piezoelectric coupling observed experimentally[4]. Monoclinic phases, characterized by the polarization vector (\mathbf{P}) along low symmetry directions, were carefully analyzed and shown to be relevant to the large piezoelectricity in 92%PbZn_{1/3}Nb_{2/3}O₃-8%PbTiO₃ [5] and also found in another technologically important ferroelectric, Pb(Zr_xTi_{1-x})O₃[6].

Interestingly, piezoelectric response of BaTiO₃ (a simple, classic ferroelectric) was shown to be enhanced significantly by crystallographically engineering single crystals through applied DC bias[7, 8]. This involves nonlinear response of BaTiO₃ and is linked with electric field induced structural phase transitions[4, 5, 9] in ferroelectrics. Polarization switching, crucial to memory applications, is another closely related nonlinear phenomenon whose microscopic mechanism is yet to be uncovered. Understanding of these nonlinear phenomena within a single picture is facilitated by knowledge of electric field-temperature phase diagrams of a ferroelectric.

Using phenomenological Landau-Ginzburg-Devonshire theory, electric field-temperature ($E - T$) phase diagrams have been studied for single crystal BaTiO₃, showing evidence for monoclinic phases[10]. Similarly, it was shown in general by Vanderbilt and Cohen [11] that the extension of the sixth order Devonshire theory to eighth and twelfth orders in polarization as the order parameter was necessary to explain the presence of stable monoclinic and triclinic phases, respectively.

Here, we present molecular dynamics simulations carried out for a comprehensive investigation of polarization switching in BaTiO₃ through determination of (a) its temperature dependence, (b) paths followed during switching with field along different directions, and (c) detailed electric field-temperature phase diagrams. This permits identification of different monoclinic phases that are stabilized as a function of electric field and temperature, and are relevant to both ultra-high piezoelectric response and polarization switching properties.

We use a first-principles effective Hamiltonian in classical molecular dynamics simulations that (1) capture most nonlinearities by construction, and (2) include thermal fluctuations in polarization and strain. A similar approach has been used earlier[12] in finding polarization paths as a function of applied field at a fixed temperature. An effective Hamiltonian H_{eff} is a Taylor series expansion of the energy surface around the high symmetry cubic perovskite structure, written in terms of the low energy local degrees of freedoms (DoFs), three acoustic phonon modes (which capture the physics of inhomogeneous strain) and three low energy (soft) optical phonon modes (which give local dipole moments). In order to include effects of an external electric field on the system, a term $-Z^* \sum \mathcal{E} \cdot u(R)$ where Z^* and $u(R)$ are the Born effective charge and displacement associated with the soft-mode variable of the unit cell at R , is added to H_{eff} . We use parameters in H_{eff} as determined in Refs [14] and [15] from first-principles density functional theory calculations with local density approximation (LDA). Use of LDA causes an underestimation of the lattice parameter, hence a negative pressure of -5 GPa is applied to all systems simulated [15] here.

Mixed space molecular dynamics[16, 17] (MD) is used here to determine finite temperature properties of H_{eff} with periodic boundary conditions. The FERAM code used in our simulations is described in detail in Ref[19] and the program can be downloaded from <http://lotto.sourceforge.net/feram>. In order to simulate polarization hysteresis, the temperature is first increased or decreased in steps of ~ 30 K to achieve an equilibrium at the temperature of the hysteresis simulation. Then, at fixed temperature, the electric field is switched on from zero to a positive value E_{max} , from which it is decreased to $-E_{\text{max}}$ in steps of about 10 kV/cm to 100 kV/cm. Subsequently, it is again increased finally to E_{max} to obtain a complete hysteresis loop. At each temperature (and electric field), the system is thermalized for initial 70,000 timesteps and then averaging is performed over the next 30,000 timesteps, amounting to a simulation period of 0.2 ns.

For the high temperature cubic paraelectric phase, we simulate response to electric field

TABLE I: Parameters in the Langevin function used in fitting $P(E)$ data of the paraelectric phase at different temperatures.

T (K)	k_1 (C/m ²)	k_2 (Cm $\times 10^{-5}$)
400	0.12	25.4
370	0.12	41.5
340	0.11	101.8

applied along [001] direction (symmetry would give the same response to fields along other directions). The Langevin function

$$L(E) = k_1 \left[\coth \frac{k_2 E}{k_B T} - \frac{k_B T}{k_2 E} \right] \quad (1)$$

describes fairly well the $P(E)$ curves of the paraelectric phase (see Fig 1a and fitting parameters k_1 and k_2 in Table 1). While k_1 , which relates to the saturated polarization remains roughly constant, k_2 , which is proportional to the dielectric constant of the paraelectric phase, diverges as T approaches T_c ($T \leftrightarrow C$). Almost perfect fits to $P(E)$ curves of the paraelectric phase with just two parameters and their expected temperature dependence validates our MD simulations to study further these nonlinear hysteresis properties of the polar phases.

For polar phases, we simulate response to field applied (a) along the respective polar axis and (b) along other high symmetry crystallographic directions (eg., along [101] direction of the tetragonal phase where \mathbf{P} points along [001]). Generally, the magnitude of field at which switching occurs, \mathcal{E}_c , reduces as the temperature increases upto the transition to higher temperature phase (see results for tetragonal and rhombohedral phases in Fig 1b and 1c).

We now focus on the direction-dependence of polarization switching in rhombohedral phase. We find that the coercive field \mathcal{E}_c when applied along [001] direction is almost a factor of 5 smaller than that when applied along [111] direction. While the reduction in \mathcal{E}_c with T can be readily understood through the concept of lowering of Landau free energy barrier near the transition, a strong dependence of \mathcal{E}_c on its direction is related to the fact that transition state itself could be different.

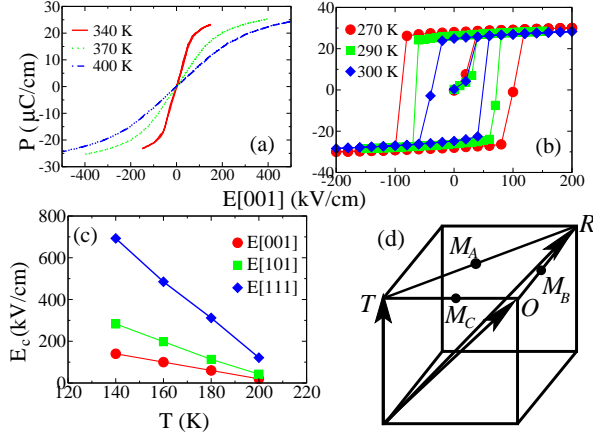


FIG. 1: (Color online) Average value of polarization P_z as a function of electric field E for (a) cubic paraelectric and (b) tetragonal ferroelectric phases when electric field is applied along $[001]$ direction. (c) Coercive field \mathcal{E}_c as a function of temperature for fields along $[111]$, $[101]$ and $[001]$ directions respectively, applied to rhombohedral phase. (d) Cohen's Cube depicting the high symmetry tetragonal (T), orthorhombic (O) and rhombohedral (R) phases and monoclinic M_A , M_B and M_C phases.

In order to investigate the transition states relevant to switching, we examine the paths followed by the system during polarization switching. When E is parallel to \mathbf{P} , the path is linear (\mathbf{P} to $-\mathbf{P}$) by symmetry. We use the following nomenclature to describe the different phases encountered along the polarization paths (Fig. 2): T, O and R denote the tetragonal, orthorhombic and rhombohedral phases respectively, and, M_A , M_B and M_C denote the three different monoclinic phases as defined in Ref.[11]. In the M_C phase, \mathbf{P} points along $[0uv]$ ($u \neq v$), and in the M_A and M_B phases \mathbf{P} points along $[uuv]$, with $u < v$ and $u > v$, respectively. The monoclinic phases are also illustrated with the Cohen's cube[3] (see Fig. 1d).

With field along $[001]$ and $[111]$ directions, switching in the orthorhombic phase (at 240 K) occurs through monoclinic phases M_C and M_B that appear along the path at 25 kV/cm and $15\sqrt{3}$ kV/cm, respectively. The transition from orthorhombic to the respective monoclinic phases is marked by (1) a jump in the polarization path from point 1 to 2 in Fig. 2a and 2b, and (2) a change in the slope of the curve of eigenvalues η of strain tensor as a function of electric field (Fig. 3a and 3b). The second crossover ($M_C \rightarrow T$ and $M_B \rightarrow R$) manifests as a change in the slope of η at ~ 60 kV/cm (Fig. 3a) and ~ 50 kV/cm (Fig. 3b), respectively. The sequence of phases, $O \rightarrow M_C \rightarrow T$ (Fig. 2a) and $O \rightarrow M_B \rightarrow R$ (Fig. 2b) can be readily

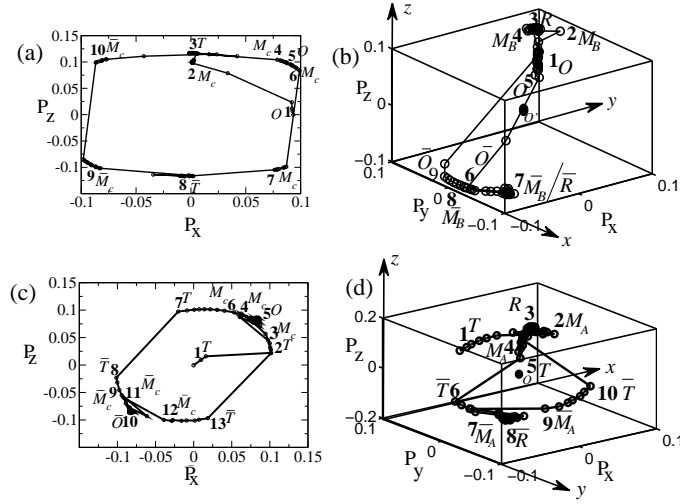


FIG. 2: Paths of polarization traced during switching when field is applied along (a) [001] and (b) [111] directions to orthorhombic phase at 240 K and (c) [101] and (d) [111] directions to tetragonal phase at 290 K. The numbers mark the sequence of phases (nomenclature in the text) followed by **P**.

rationalized through continuous paths along the Cohen's cube (see Fig. 1d).

Along the polarization paths for tetragonal phase (at 290 K), the monoclinic phases M_C and M_A emerge when fields point along [101] (Fig. 2c) and [111] (Fig. 2d) directions, respectively. The transitions from tetragonal to the monoclinic phases are evident in the changing slopes at ~ 40 kV/cm of η (Fig. 3c and 3d). Only at higher fields ~ 100 kV/cm, close to E_{max} , the phases become orthorhombic and rhombohedral, respectively. The sequence of phases $T \rightarrow M_C \rightarrow O$ and $T \rightarrow M_A \rightarrow R$ also follows from Cohen's cube (Fig. 1d).

At a field of 25 kV/cm along [001] direction of the orthorhombic phase, there occurs a jump (from point 6 to 7 in Fig. 2a) along the path of switching which corresponds to a rotation from M_C to \bar{M}_C . Similarly when the field is $15\sqrt{3}$ kV/cm along [111] direction, a jump from point 5 to 6 (see Fig 2b) corresponds to a rotation from O to \bar{O} . Both the switching fields are lower compared to \mathcal{E}_c of $40\sqrt{2}$ kV/cm along [101] direction. In the tetragonal phase as well, switching from T to \bar{T} occurs at the field of $25\sqrt{2}$ kV/cm along [101] direction, as revealed by jump from point 7 to 8 in Fig. 2c, and at the field of $15\sqrt{3}$ kV/cm along [111] direction as revealed by a jump from point 5 to 6 in Fig. 2d; both \mathcal{E}_c 's are much lower than the coercive field of $\mathcal{E}_c = 60$ kV/cm along [001] direction. Thus, our finding for

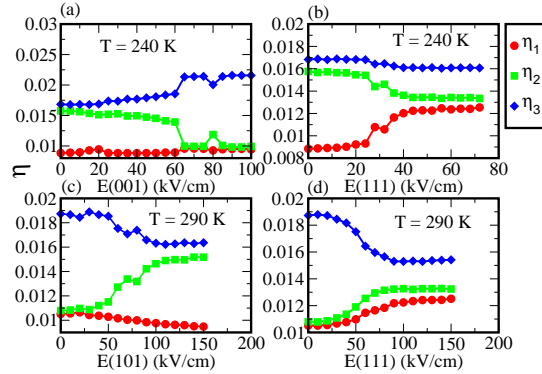


FIG. 3: (Color online) Eigenvalues η of strain tensor as a function of field applied along (a) [001] (b) [111] directions to the orthorhombic phase at 240 K and (c) [101] (d) [111] directions to the tetragonal phase at 290 K.

the rhombohedral phase (Fig. 1c), is also seen to be true for orthorhombic and tetragonal phases: switching with fields applied along polar direction occurs at much higher fields than that applied along other crystallographic directions. While the polarization rotation[3] through monoclinic phases (which are known to be present near the morphotropic phase boundaries [5, 12, 13]) has been shown to be responsible for giant piezoelectric response, we show that it facilitates polarization switching at lower fields and is crucial for memory applications.

We further investigate the existence and thermodynamic stability of monoclinic phases through $E - T$ phase diagrams. The electric field is turned on at the beginning of the simulations, and is kept constant. The temperature is then increased (decreased) in order to perform heating (cooling) simulations which give the polarization, and dielectric susceptibility as a function of temperature. We simulated temperature dependent phase transitions for fields along [001], [101] and [111] directions varying from 10 kV/cm to 100 kV/cm in steps of 5 kV/cm. The contour plots of eigenvalues of dielectric tensor as a function of field and temperature naturally give a picture of the electric field - temperature ($E - T$) phase diagrams (Fig. 4). As the peak in dielectric constant marks a transition, high density of contours visible clearly as dark regions resembling thick lines/curves (Fig 4) mark the phase boundaries in $E - T$ phase diagrams. These lines meet T-axis at 320 K, 250 K and 220 K at $E = 0$, which are the transitions temperatures in zero electric field[20]. Hysteresis in heating and cooling simulations give small errors (~ 10 K and 10 kV/cm) in the phase boundaries .

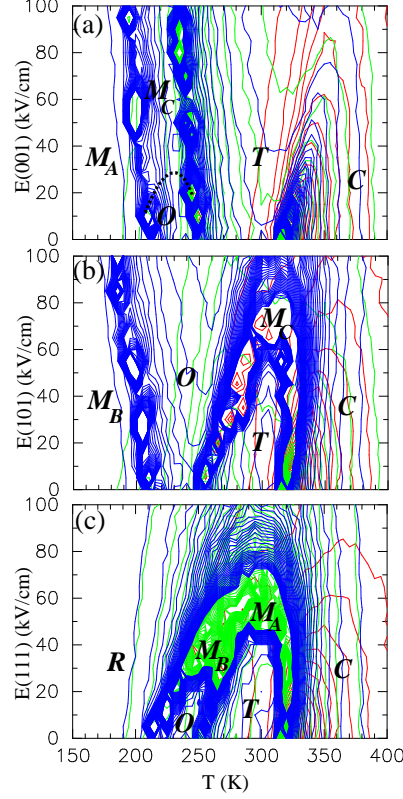


FIG. 4: (Color online) $E - T$ phase diagrams expressed as contour plots of eigenvalues of the dielectric tensor. High density of contours near the peak values of dielectric response give rise to thick and dark lines which form the boundaries between different stable phases. A crossover from one phase to another at such a boundary is also seen as a discontinuity in the slope of $\eta(E)$ in Fig. 3.

For field along [001] direction, there is no qualitative change in the phase transition behavior with increasing field (Fig 4a); the temperature range of the stable tetragonal phase expands with field. We note that a nonzero field breaks the symmetry of the system and the transition from C to T phase becomes diffused, and above the field of 50 kV/cm, there is virtually no difference between the T and C phases. The orthorhombic phase transforms to monoclinic M_C phase above a field of about 30 kV/cm, as characterized by a change in the slope of strain as a function of electric field (see Fig. 3). When the field is applied along the [101] direction, the temperature interval of the stable orthorhombic phase expands with field. The tetragonal phase transforms through an intermediate monoclinic M_C phase to an orthorhombic phase above $80\sqrt{2}$ kV/cm. Boundaries of the region of stability of the M_C phase are characterized by peaks in eigenvalues of dielectric response appearing as

thick dark lines (see Fig. 4b). Similarly for field along [111] direction, both tetragonal and orthorhombic phases transform at fields of about $40\sqrt{3}$ and $20\sqrt{3}$ kV/cm to M_A and M_B phases, respectively. Above the field of $60\sqrt{3}$ kV/cm, there is no clear boundary between rhombohedral and cubic phases. The lines of transition from monoclinic phases to T, O and R phases (with increasing fields) in our $E - T$ phase diagrams are topologically similar to those in Bell's work[10] based on phenomenological theory and even the fields of these transitions agree within $\sim 20\%$ with Bell's estimates. However, our phase diagram differs in an important way: the region of stable monoclinic phases appears only above nonzero electric fields and its boundary with T , O and R phases at lower fields is characterized by (a) peak in the dielectric response (Fig. 4) and (b) change in the slope of η changes (Fig. 3).

The sequence of phases appearing along the switching paths followed by the system during **P-E** hysteresis can be understood from the constant temperature lines in the $E - T$ phase diagrams. For example, applying field along [111] direction of the tetragonal phase at 290 K would result in **P** tracing the path described in Fig. 2d. The connectivity between different monoclinic phases and T , O , R phases in the $E - T$ phase diagram is consistent with that obtained from the Cohen's cube[3]. The change in the slope of strain as a function of field (see Fig 3) at a crossover from a T or O or R phase to a monoclinic one gives rise to the giant piezoelectric response arising at finite fields in experiments[7, 8].

To summarize, we have used effective hamiltonian in molecular dynamics simulations and have shown that: (1) switching fields are highest for the cases when the external electric field is applied along the direction of the polar axis, (2) switching occurs at low values of fields along other directions because of the polarization rotation through monoclinic phases. Stability of these monoclinic phases has been carefully analysed through determination of the $E - T$ phase diagrams, which should be fundamental to the design of both electromechanical and memory type of devices.

J.P. thanks CSIR and T.N. thanks JNCASR, MEXT-Japan and JSPS. We acknowledge helpful discussions with Dhananjai Pandey and Subir K Das. We thank the CCMS super-computing facility at JNCASR.

[1] M. Dawber, K. M. Rabe, J. F. Scott, Reviews of Modern Physics, **77**, 1083 (2005)

- [2] J. F. Scott, C. A. P. de Araujo, *Science* **246**, 1400 (1989)
- [3] H. Fu, R. E. Cohen, *Nature* **403**, 281 (2000)
- [4] S-E. Park, T. R. Shrout, *J. Appl. Phys.* **86**, 1804 (1997)
- [5] B. Noheda, D. E. Cox, G. Shirane, S-E. Park, L. E. Cross, Z. Zhong, *Phys. Rev. Lett.* **86**, 3891 (2001)
- [6] S. K. Mishra, D. Pandey, A. P. Singh, *Appl. Phys. Lett.* **69**, 1707 (1996)
- [7] S. Wada et al., *Jpn. J. Appl. Phys.* **38**, 5505 (1999)
- [8] S-E. Park, S. Wada, L. E. Cross, T. R. Shrout, *J. Appl. Phys.* **86**, 2746 (1999)
- [9] D-S. Paik, S-E. Park, S. Wada, L. E. Cross, T. R. Shrout, *J. Appl. Phys.* **86**, 2746 (1999)
- [10] A. J. Bell, *J. Appl. Phys.* **89**, 3907 (2001)
- [11] D. Vanderbilt, M. H. Cohen, *Phys. Rev. B* **63**, 094108 (2001)
- [12] L. Bellaiche, A. Garcia, D. Vanderbilt, *Phys. Rev. B* **64**, 060103(R) (2001)
- [13] B. Noheda, Z. Zhong, D. E. Cox, G. Shirane, S-E. Park, P. Rehrig, *Phys. Rev. B* **65**, 224101 (2002)
- [14] W. Zhong, D. Vanderbilt, K. M. Rabe, *Phys. Rev. Lett.* **73**, 1861 (1994)
- [15] W. Zhong, D. Vanderbilt, K. M. Rabe, *Phys. Rev. B* **52**, 6301 (1995)
- [16] U. V. Waghmare, E. J. Cockayne, B. P. Burton, *Ferroelectrics* **291**, 187 (2003)
- [17] B. P. Burton, E. J. Cockayne, U. V. Waghmare, *Phys. Rev B* **72**, 064113 (2005)
- [18] S. D. Bond, B. J. Leimkuhler, B. B. Laird, *J. Comput. Phys.* **151**, 114 (1999)
- [19] T. Nishimatsu, U. V. Waghmare, Y. Kawazoe, D. Vanderbilt, arXiv:0804.1853v2 [cond-mat.mtrl-sci](To be published in *Phys. Rev. B*)
- [20] J. Paul, T. Nishimatsu, Y. Kawazoe, U. V. Waghmare, *Phys. Rev. Lett* **99**, 077601 (2007)